Environmental Science
Advances

PAPER

View Article Online
View Journal | View Issue

Cite this: *Environ. Sci.: Adv.*, 2024, **3**, 44

Polyamidoxime (PAO) granules for solar-enhanced uranium extraction from seawater†

Xue Zhang, Qianhong Gao and Dadong Shao *

Received 1st July 2023
Accepted 10th November 2023

DOI: 10.1039/d3va00179b

rsc.li/esadvances

Extracting uranium (U(VI)) from seawater can effectively solve the shortage of uranium resources on land. The key to U(VI) extraction from seawater is preparing high performance U(VI) extraction materials. Although PAO based materials present outstanding performance in U(VI) extraction, their experimental adsorption capabilities are greatly restricted by its aggregation. To inhibit PAO aggregation, we used $KMnO_4$ as a regulator to interfere with PAO aggregation in aqueous solutions, and the physicochemical properties of the obtained $KMnO_4$@PAO were well characterized. Importantly, $KMnO_4$@PAO also presents excellent photo-thermal conversion properties in various aqueous solutions, which are beneficial for U(VI) extraction. The adsorption properties of $KMnO_4$@PAO for U(VI) under different solution conditions (pH, adsorption time, U(VI) ion concentration, and temperature) were studied by batch adsorption experiments. The results reveal that $KMnO_4$@PAO presents excellent adsorption properties for U(VI), and its efficient photo-thermal conversion properties can increase solution temperature and U(VI) adsorption capability.

Environmental significance

Uranium is the fundamental material of nuclear energy and is a representative actinide element of radioactive wastewater management. The immobilization and enrichment of uranium from aqueous solutions is an important for nuclear energy.

Introduction

Nuclear energy is a vital part of the solution to global climate change especially under the current "two-carbon" target.[1,2] Uranium is the primary material of nuclear energy, and terrestrial uranium ore is limited and will be exhausted in a few decades. The search for new uranium source is critical for the future of nuclear energy. The ~4.5 billion tons of U(VI) in seawater is a thousand times that in terrestrial ore.[3–6] Meanwhile, ~27 000 tons of U(VI) is also replenished by rivers yearly.[7,8] How to extract U(VI) from seawater has become a research hotspot, and many schemes, including chemical precipitation, evaporation, ion exchange, and membrane separation, have been reported for U(VI) extraction from seawater.[9–14] Adsorption is widely regarded as one of the promising strategies for this target owing to its merits, such as simple operation and environmentally friendly process.[15–20] After decades of research, people found that the material is one core of this task, directly determining the efficiency and comprehensive cost of U(VI) extraction. Developing materials with excellent comprehensive and economy properties is significant for U(VI) extraction.

Amidoxime (AO, $-C(NH_2)=N-OH$) contains both an oxime group and amino group, and the oxygen atom in the oxime group and the nitrogen atom in the amino group both contain free lone electron pairs. Therefore, it is easy for AO to form stable complexes with U(VI) ions,[21–23] and it has become an indispensable part of various U(VI) extraction materials. The excellent stability of PAO based materials has been tested in seawater.[17,23–26] Polyacrylonitrile (PAN) is widely used as the precursor for PAO because the core $-C\equiv N$ in PAN can be easily converted into AO. Many methods are used to convert PAN into PAO, NH_2OH amidoximation is the most classic method.[27–31] NH_2OH amidoximation technique includes homogeneous and heterogeneous methods, which were react in organic solvents[31–33] and in aqueous solutions,[28,34] respectively. Organic solvents used in the homogeneous method result in environmental pollution and high cost, which dramatically reduces the comprehensive competitiveness of PAO in U(VI) extraction. Meanwhile, PAN quickly settles down in aqueous solution, and most $-C\equiv N$ in PAN cannot react with NH_2OH in the heterogeneous method.

To inhibit PAN aggregation in aqueous solutions during the NH_2OH amidoximation process, a new strategy is developed in this work by using $KMnO_4$ as a regulator. The added $KMnO_4$ can

---

School of Environmental and Biological Engineering, Nanjing University of Science and Technology, Nanjing 210094, PR China. E-mail: shaodadong@126.com

† Electronic supplementary information (ESI) available. See DOI: https://doi.org/10.1039/d3va00179b

effectively inhibit PAN agglomeration, regulate PAN morphology, and endow PAO with photo-thermal properties. The adsorption and photo-thermal conversion properties of $KMnO_4$@PAO in a variety of aqueous solutions, including ultrapure water, tap water, river water, and simulated seawater, have been systematically studied. This method can reduce the cost of PAO-based materials, in line with the concept of green development.

Results and discussion

Characterization

Fig. 1A shows the synthesis procedure and U(VI) adsorption of $KMnO_4$@PAO. PAN as a macromolecule will undergo intramolecular agglomeration in aqueous solution and settle down as a block before reacting with NH_2OH. Ultimately, it limits the application of PAO based materials in U(VI) recovery performance. In this work, we successfully suppressed the agglomeration of PAO in aqueous solution by using $KMnO_4$ as a regulator, and the obtained $KMnO_4$@PAO is uniform in aqueous solution (Fig. 1B). Particle size distributions of PAO and $KMnO_4$@PAO were also studied by DLS measurement. Compared with PAO, the size of $KMnO_4$@PAO is significantly decreased, and the diameters of PAO and $KMnO_4$@PAO were concentrated at ~1100 nm (Fig. 1C) and ~400 nm, respectively. In a word, the PAO particle size can be easily adjusted by using $KMnO_4$.

SEM was used to investigate the effect of $KMnO_4$ and PAO amounts on the surface morphology of $KMnO_4$@PAO. PAO amount did not shown significant impact on PAN surface topologies when the $KMnO_4$ dosage was fixed at 0.20 g (Fig. 2A and B), whereas the agglomeration of PAO apparently increases with increasing $KMnO_4$ amount when the PAO dosage was fixed at 2.0 g (Fig. 2C and D). When $KMnO_4$ is introduced into the suspensions of PAN and NH_2OH, the redox reaction between NH_2OH and $KMnO_4$ and the conversion of –C≡N to –C(NH_2)=N–OH coexist together, which restricts and promotes each other in aqueous solutions. The reaction is dominated by solution compositions. At low PAN $KMnO_4$ content, the primary reaction in the solution is the amidoximation of PAN and NH_2OH. The present $KMnO_4$ can inhibit the generation of unsaturated amines, and finally obtain uniformly dispersed PAO particles. At high $KMnO_4$ content, the dominating reaction in the solution is the reduction reaction of $KMnO_4$ and NH_2OH. Few –C≡N was reduced by NH_2OH, and the unreacted –C≡N bond to each other to form unsaturated amine, and settle down in aqueous solution. It means that the morphology and size of $KMnO_4$@PAO can be easily adjusted by controlling $KMnO_4$ amounts. The $KMnO_4$@PAO prepared with 2.0 g PAO and 0.20 g $KMnO_4$ shows ideal morphology and size, and is selected for subsequent experiments.

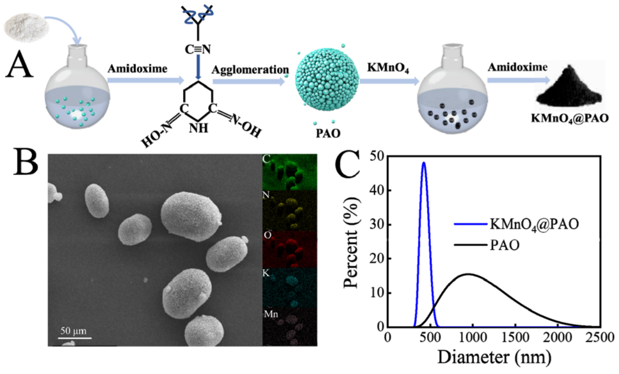

Fig. 1 Diagram of $KMnO_4$@PAO synthesis procedures (A); SEM images – EDS maps of $KMnO_4$@PAO (B); size distributions of PAO and $KMnO_4$@PAO (C).

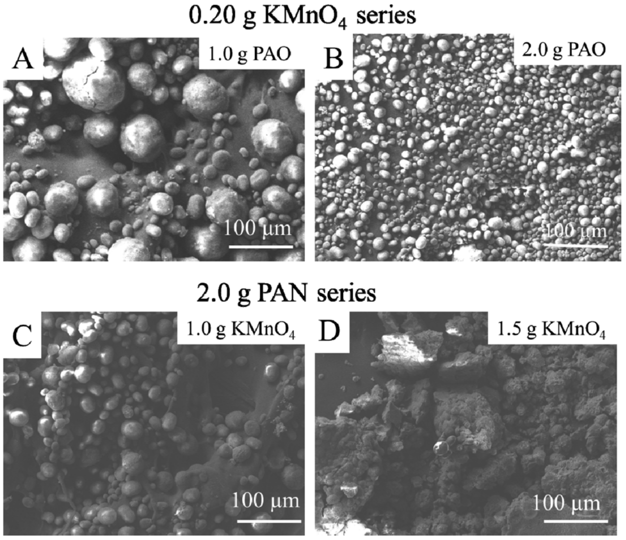

Fig. 2 SEM images of $KMnO_4$@PAO with different $KMnO_4$ and PAO amounts. 0.20 g $KMnO_4$ series: 1.0 g PAO (A); 2.0 g PAO (B). 2.0 g PAN series: 1.0 g $KMnO_4$ (C); 1.5 g $KMnO_4$ (D). The details of $KMnO_4$@PAO preparation conditions are shown in Table S1.†

The FT-IR technique was used to study the effects of $KMnO_4$ on the surface functional groups and thermal stability of $KMnO_4$@PAO. As shown in Fig. 3A, the weak FT-IR band at

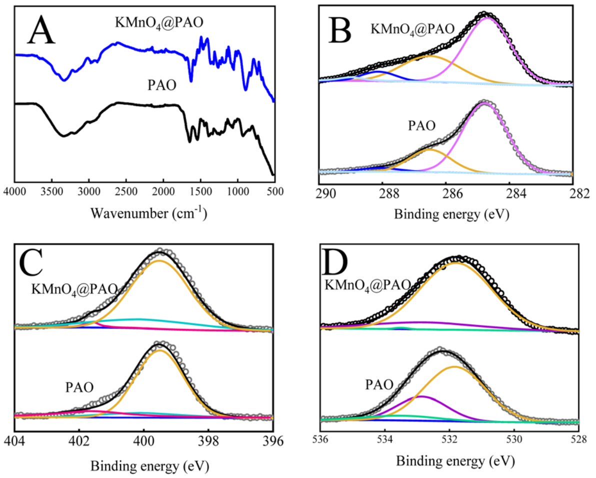

Fig. 3 FT-IR (A), C 1s (B), N 1s (C), and O 1s (D) spectra of $KMnO_4$@PAO and PAO.

~2240 cm^{-1} is related to stretching vibration of residual –C≡N groups in PAO and $KMnO_4$@PAO. The peaks at ~1651 and ~932 cm^{-1} can be respectively assigned to –C=N and N–O vibrations, which reveals the high conversion of PAN to PAO.[17,23] The FT-IR spectrum results show that the introduced $KMnO_4$ cannot significantly affect the conversion of PAN to PAO during the amidoximation process.[35]

The functional groups on PAO and $KMnO_4$@PAO surfaces are verified by XPS spectroscopy. The XPS peaks of O 1s, N 1s, and C 1s were located at ~532 eV, ~400 eV, and ~285 eV, respectively.[36] The XPS C 1s[15,36] spectra of $KMnO_4$@PAO and PAO can be deconvoluted into four peaks at 284.8 ± 0.1 eV, 286.5 ± 0.1 eV, 288.1 ± 0.1 eV and 288.9 ± 0.1 eV, which can be assigned to –C≡N, C–OH, –C=O, and –COOH, respectively. The proportion of –C≡N in $KMnO_4$ is significantly lower than that of PAO, indicating the higher conversion of PAN in $KMnO_4$@PAO (Fig. 3B, Table S2†). PAO-based materials present excellent stability,[23–26] The content of –COOH increases after adding $KMnO_4$ during the conversion of PAN to PAO. It is speculated that $KMnO_4$ works as an oxidant in the solution, and MnO_2 is its product. MnO_2 can catalyze the transformation of –C≡N into –C(NH_2)=N–OH, and promote the hydrolysis of –C≡N to –COOH in the presence of NaOH.[18]

The XPS N 1s[6,16] spectra of $KMnO_4$@PAO and PAO (Fig. 3C, Table S3†) can be deconvoluted into three species at 399.5 ± 0.1 eV, 400.0 ± 0.1 eV, and 401.6 ± 0.1 eV, which were attributed to N–H, H_2N–C=NOH, and $-N^+$, respectively. As shown in Table S3,† the content of H_2N–C=NOH in $KMnO_4$@PAO is significantly higher than that in PAO. The results of XPS C 1s and N 1s spectra reveal that more PAN was converted into PAO by $KMnO_4$@PAO. The XPS O 1s[6,23] spectra of $KMnO_4$@PAO and PAO could be deconvoluted into three peaks of –COOH at 581.8 ± 0.1 eV, C=O at 532.8 ± 0.1 eV, and –OH at 533.5 ± 0.1 eV (Fig. 3D, Table S4†). The identical XPS results of PAO and $KMnO_4$@PAO indicate that their chemical bonding environments are similar. The introduced $KMnO_4$ has no significant effect on the chemical environments of PAO.

U(VI) adsorption capability

Solution pH influences adsorption behavior by affecting the existing forms of U(VI) in solution and the surface charge of the adsorbent. Fig. 4A exhibits the adsorption capacities and zeta potentials of $KMnO_4$@PAO at different pH values.[23,30,31] The adsorption capacity gradually increases with increasing pH to 5, and then gradually decreased with further increasing pH. The $KMnO_4$@PAO surface is positively charged due to protonation at pH < 5, and U(VI) is predominantly present as positively charged free UO_2^{2+}. The strong electrostatic repulsion between $KMnO_4$@PAO and UO_2^{2+} results in low adsorption capacity. With increasing solution pH, the protonation level of the $KMnO_4$@PAO surface gradually decreases, which benefits U(VI) adsorption. At pH > 5.0, negatively charged U(VI) species (such as $UO_2(OH)_3^-$) appear, and the $KMnO_4$@PAO surface becomes negatively charged. Again, the electrostatic repulsion results in low adsorption capacity.

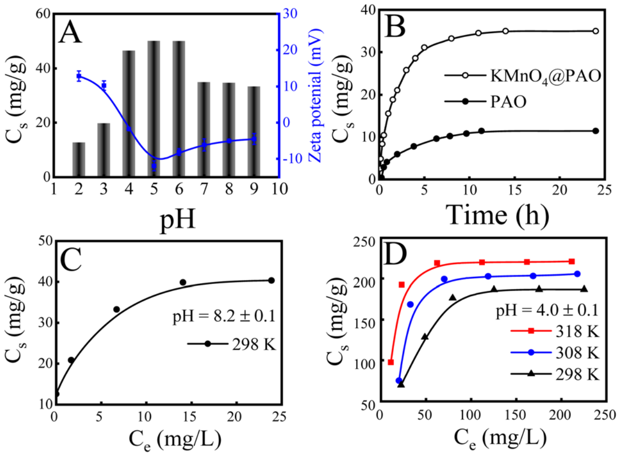

Fig. 4 Effect of pH on zeta potential of $KMnO_4$@PAO for U(VI) (A); effect of pH (A) and contact time on adsorption capability of $KMnO_4$@PAO for U(VI) (B); adsorption isotherms of U(VI) on $KMnO_4$@PAO and on PAO at pH = 8.2 ± 0.1 (C) and at pH = 4.0 ± 0.1 (D). $m/V = 0.4$ g L^{-1}, $I = 0.1$ mol per L NaCl. (A) $T = 298 \pm 1$ K, contact time: 24 h, $C[U(VI)]_{initial} = 20$ mg L^{-1}, pH = 8.2 ± 0.1. (B) $T = 298 \pm 1$ K, $C[U(VI)]_{initial} = 20$ mg L^{-1}, pH = 8.2 ± 0.1. (C) $T = 298$ K ± 1 K, contact time: 24 h, pH = 8.2 ± 0.1. (D) Contact time: 24 h, pH = 4.0 ± 0.1.

The effect of contact time on the extraction of U(VI) by $KMnO_4$@PAO is also studied, and the result is shown in Fig. 4B. Due to the abundant adsorption sites, the adsorption of U(VI) on $KMnO_4$@PAO rapidly increases with increasing contact time in the initial 5 h. The adsorption sites are gradually exhausted with the progress of the reaction, and the adsorption reaction slowly reaches an equilibrium. To deeply understand the adsorption process, pseudo first order and pseudo second order kinetic models[4,6] are used to analyse kinetic adsorption data, and the relevant results are shown in Fig. S1 and Table S5.† According to the correlation coefficients (R^2), the pseudo second order model is more suitable to describe the adsorption of U(VI) on the $KMnO_4$@PAO surface, indicating that the enrichment of U(VI) on the $KMnO_4$@PAO surface is a chemisorption process. From the pseudo second order model fitting results, the maximum adsorption capacities of U(VI) on $KMnO_4$@PAO were 38.4 mg g^{-1} at pH 8.2 and 298 K, about 3 times that of PAO (13.1 mg g^{-1}) under the same conditions. Results show that $KMnO_4$ not only inhibits PAO agglomeration but also improves PAO adsorption capability. It further enhances the competitiveness of PAO as a candidate for U(VI) extraction from seawater.

The maximum adsorption capacity of $KMnO_4$@PAO for U(VI) was explored by the adsorption isotherm technique at pH 8.2 and 298 K (Fig. 4C), and the adsorption data were analysed by commonly used Langmuir and Freundlich models (Fig. S2A†). According to the R^2 values in Table S6,† the Langmuir model was more suitable to describe the adsorption process than the Freundlich model, demonstrating that adsorbed U(VI) was chemisorbed and formed a single layer on the $KMnO_4$@PAO surface.[26–28] After the addition of $KMnO_4$, the adsorption capacity is significantly increased. This means that except PAO, the manganese related compounds in $KMnO_4$@PAO can also recover U(VI), which can significantly solidify U(VI) in acidic solutions.[37,38] To further expand the application scope of $KMnO_4$@PAO, we explored the adsorption of $KMnO_4$@PAO at pH 4. Experimental results show that $KMnO_4$@PAO has good curing ability for U(VI), which benefits the application of PAO-based materials in wastewater management. To evaluate the maximum adsorption capacity ($C_{s,max}$) and the related thermodynamic parameters of $KMnO_4$@PAO for U(VI) in acidic solutions, the adsorption isotherms of U(VI) on $KMnO_4$@PAO were obtained at pH 4.0 and 298–318 K (Fig. 4D). The adsorption capacity of $KMnO_4$@PAO for U(VI) gradually increases with increasing $C[\text{U(VI)}]_{\text{initial}}$ and solution temperature. The $C_{s,max}$ value of $KMnO_4$@PAO is 233 mg g^{-1} at 298 K and pH 4, which is competitive to hot materials (Table 1).

The experimental data were also fitted by the commonly used Langmuir and Freundlich models (Fig. S2B†), and the obtained fitting parameters are shown in Table S7.† The R^2 values indicate that the Langmuir model again better describes the adsorption process of U(VI) on $KMnO_4$@PAO in acidic solutions than the Freundlich model. Determining thermodynamic parameters (standard enthalpy change $\Delta H°$, standard Gibbs free energy change $\Delta G°$, and entropy change $\Delta S°$) is very important for the effective evaluation of adsorption properties.[36] The thermodynamic parameters for U(VI) adsorption on $KMnO_4$@PAO are calculated and shown in Table S8.† The positive $\Delta H°$ value, positive $\Delta S°$ value, and negative $\Delta G°$ value indicate that U(VI) adsorption on thr $KMnO_4$@PAO surface is a spontaneous and endothermic process. The positive $\Delta H°$ value reveals that increasing reaction temperature is conducive to the adsorption reaction, which is consistent with macroscopic experimental results.

Repeatability and stability are essential indices to evaluate the availability of the adsorbent. To screen suitable eluants for $KMnO_4$@PAO, the effect of eluant type (0.1 mol L^{-1}) on U(VI) desorption from the $KMnO_4$@PAO surface was investigated. As shown in Fig. S3,† Na_2CO_3 shows a particularly prominent elution effect on U(VI) among the studied eluants ($NaCO_3$, $NaHCO_3$, NaOH, HCl, and HNO_3).[25] Na_2CO_3 is often used to elute U(VI), and the elution rates can reach 80–100%.[5,11,13,19] So Na_2CO_3 is selected as the eluant in the cyclic experiment. U(VI) elution increases to ~100% on increasing $C[Na_2CO_3]$ to 0.5 mol L^{-1}, and then the high level is retained (Fig. 5A). So, 0.5 mol per L Na_2CO_3 is selected for the following elution process. As shown in Fig. 5B, the adsorption capability $KMnO_4$@PAO for U(VI) only decreases ~6.1% even after 6 cycles.

Table 1 Adsorption capacities of different amino-functionalized adsorbents in U(VI) solution

Adsorbent	pH	$C_{s,max}$ (mg g^{-1})	m/V (g L^{-1})	Ref.
HCPSAN-B-AO	8.0	228	0.10	3
PCP	8.0	303	0.10	4
PAMAMG3-SDB	5.5	130	1.25	9
PCN-222-AO	7.0	552	0.20	16
PAOBS	6.0	233	0.40	17
HAPAO NFMs	6.0	409	0.005	29
$KMnO_4$@PAO	4.0	233	0.40	This work

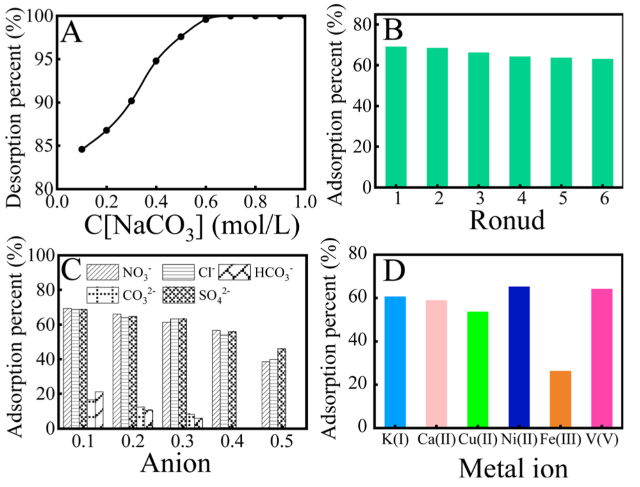

Fig. 5 Effect of Na_2CO_3 concentration on the desorption of U(VI) from $KMnO_4$@PAO (A); recycling application of $KMnO_4$@PAO in U(VI) extraction (B); effect of anions (C) and cations (D) on the adsorption capability of $KMnO_4$@PAO for U(VI). $T = 298 \pm 1$ K, contact time: 24 h, $C[\text{U(VI)}]_{\text{initial}} = 20$ mg L^{-1}, $m/V = 0.40$ g L^{-1}, pH $= 8.2 \pm 0.1$. (A), (B) and (D): $I = 0.1$ mol per L NaCl.

Seawater is a very complex ecosystem, and all known elements and compounds on earth can be found in seawater. These elements and compounds affect the recovery of U(VI) from seawater. The influence of major cations and anions in seawater on U(VI) recovery from seawater was investigated. As shown in Fig. 5C, the effect of Cl^-, NO_3^-, and SO_4^{2-} concentrations on U(VI) recovery from seawater can be neglected, whereas the recovery of U(VI) by $KMnO_4$@PAO gradually decreased with increasing HCO_3^-/CO_3^{2-} concentration. It is well known that Ca(II)/Mg(II)–U(VI)–CO_3 species are the main existing forms of U(VI) in seawater, and their dissociation is usually the determining step of U(VI) recovery.[5,11] Luckily, CO_3^{2-}/HCO_3^- concentration is stable and below 0.1 mol L^{-1} in natural seawater.[38] Since abundant competitive cations co-existed in natural seawater, the selective adsorption capacity of $KMnO_4$@PAO for U(VI) cannot be ignored.[13] As depicted in Fig. 5D, the U(VI) adsorption on the $KMnO_4$@PAO surface is much higher than that of other coexisting metals. In this work, $KMnO_4$ was used to regulate the PAO morphology. And the formed Mn related compounds have an excellent recovery effect on U(VI).[37–39] On this basis, $KMnO_4$@PAO shows high recovery capability for U(VI) against competitive cations.

Based on the excellent adsorption capability of $KMnO_4$@PAO for U(VI), the application of $KMnO_4$@PAO in extraction of U(VI) from real seawater was studied. Natural seawater was used to prepare U(VI) containing solutions with different initial concentrations. As shown in Table 2, $KMnO_4$@PAO can quantitatively take up ~50% of mg L^{-1} levels U(VI) from seawater. Experimental results further confirm the high efficiency of $KMnO_4$@PAO in extraction of U(VI) from seawater.

$KMnO_4$ may undergo photolysis and reduction reactions in aqueous solution. The products of $KMnO_4$ are depending on solution conditions when it is used as an oxidizing agent. Whatever $KMnO_4$ decomposed or reduced during the reaction,

Table 2 Selected results of U(VI) adsorption on $KMnO_4$@PAO at $m/V = 0.40$ g L^{-1}, $T = 298 \pm 1$ K, contact time: 24 h, pH 8.2 ± 0.1

C[U(VI)] (mg L^{-1})		
Initial	Final	Adsorption (%)
10	5.01	49.9
8	3.25	47.5
5	2.21	27.9
3	1.55	14.5

the resulted products are finally combined into black adsorbent powder ($KMnO_4$@PAO). Usually black objects are a heat absorber, and can effectively absorb visible light. The adsorption of U(VI) on PAO is a endothermic reaction, and the increased temperature can enhance the adsorption process. The final product black $KMnO_4$@PAO can effectively absorb sunlight and increase its temperature. This benefits the adsorption of U(VI) on $KMnO_4$@PAO surface.[26,40,41]

In summary, $KMnO_4$@PAO can work as a light conversion material that can absorb a wide range of sunlight, and the increased solution temperature further improves U(VI) recovery efficiency. As shown in Fig. 6A, after irradiation for 2 h at 0.20 W cm^{-2}, the surface temperature of $KMnO_4$@PAO increased to ~30 °C, indicating the high photo-thermal conversion properties of $KMnO_4$@PAO. The photo-thermal conversion properties of $KMnO_4$@PAO (0.40 g L^{-1}) in simulated seawater were also studied. It is incredible that just after irradiation for 2 h at 0.20 W cm^{-2}, the temperature of simulated seawater was increased to nearly ~34 °C (Fig. 6B). $KMnO_4$@PAO material can well perform the task of photo-thermal conversion, and significantly increases solution temperature. The effect of water sources (simulated seawater, ultrapure water, tap water, and river water) and light sources (simulated sunlight and infrared light) on the recovery efficiency of U(VI) by $KMnO_4$@PAO was also evaluated. According to Fig. 6C, the recovery capabilities of $KMnO_4$@PAO for U(VI) were improved under sunlight and near-infrared light irradiation. Meanwhile, the adsorption rate of U(VI) on $KMnO_4$@PAO under external light irradiation is much faster than that under dark conditions, and adsorption equilibrium is achieved in 2 h (Fig. 6D).

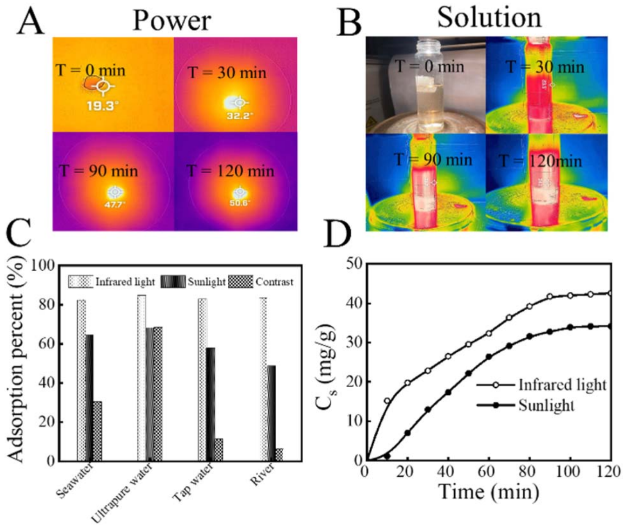

Fig. 6 Infrared images of $KMnO_4$@PAO powder (A) and 0.40 g per L $KMnO_4$@PAO suspension (B) under simulated sunlight irradiation; adsorption capability (C) and kinetics of $KMnO_4$@PAO for U(VI) under light irradiation (D). Light intensity: 0.20 W cm^{-2}. $T = 298$ K ± 1 K, contact time: 24 h, $C[U(VI)]_{initial} = 20$ mg L^{-1}, $m/V = 0.40$ g L^{-1}, pH $= 8.2 \pm 0.1$, $I = 0.1$ mol per L NaCl.

To further explore the influence of light and solution sources, the samples after the adsorption experiment were collected for FT-IR testing (Fig. 7). Experimental results show that the FT-IR spectra of $KMnO_4$@PAO under different water sources and light sources are similar, which reveal the highly stable performance of $KMnO_4$@PAO.

The used $KMnO_4$@PAO was collected to characterize morphology changes. As shown in Fig. 8A–D, $KMnO_4$@PAO can well maintain its morphology after U(VI) adsorption. EDS-mapping shows that U(VI) was uniformly adsorbed on the $KMnO_4$@PAO surface. The surface functional groups of PAO and $KMnO_4$@PAO after U(VI) adsorption were characterized by XPS spectroscopy (Fig. 8E). The adsorbed U(VI) was evidenced by the new peak at 530.80 ± 0.1 eV (Fig. 8F) related to O=U=O,[23] and the new peaks at ~390 eV (Fig. 8G) were ascribed to to XPS U 4f.[23] This reveals the high adsorption capabilities of PAO and $KMnO_4$ for U(VI). The XPS Mn 2p spectrum of $KMnO_4$@PAO can be deconvoluted into Mn 2p3/2 and Mn 2p1/2 peaks[35,37–39] at 641.78 and 653.47 eV, respectively (Fig. 8H). This confirms the successful introduction of $KMnO_4$ into PAO.

The introduced $KMnO_4$ during the PAN amidoximation process can significantly decrease PAO size from 1100 nm to 400 nm ($KMnO_4$@PAO), and solve the problem of PAO agglomeration. The introduced $KMnO_4$ also endows

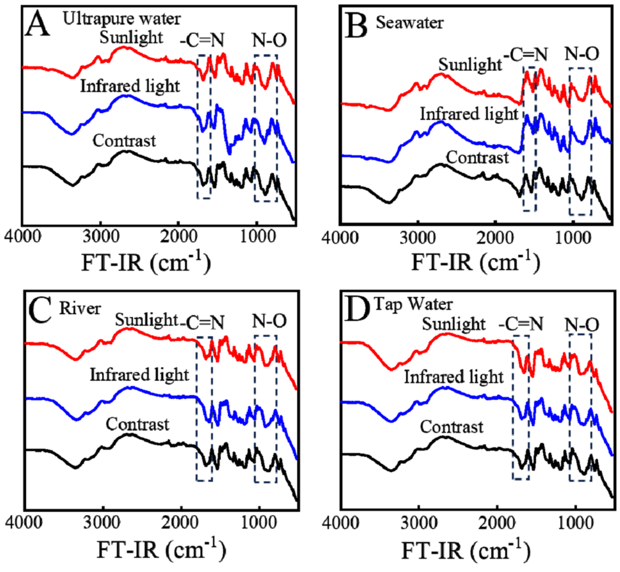

Fig. 7 FT-IR spectra of U(VI) adsorbed by $KMnO_4$@PAO under different illumination and solution conditions.

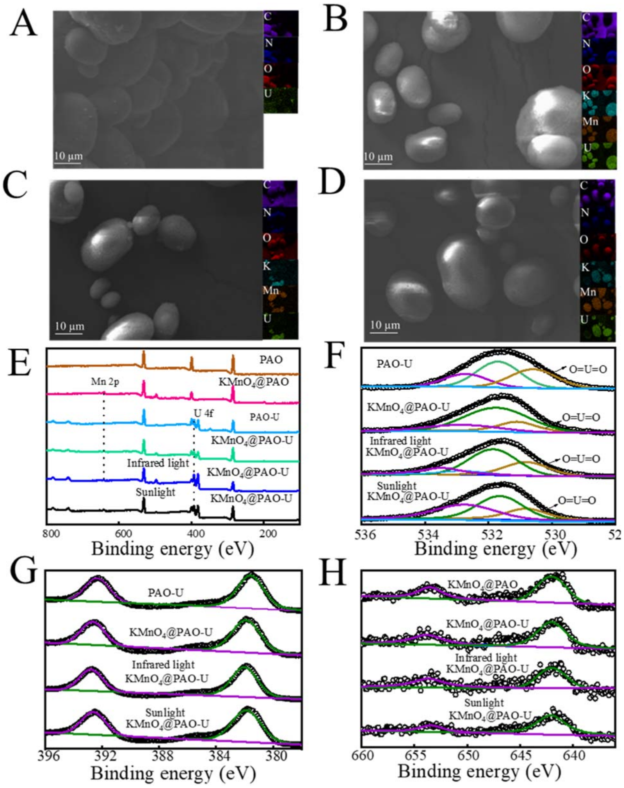

Fig. 8 SEM images of PAO-U (A), KMnO$_4$@PAO-U (B), infrared light KMnO$_4$@PAO-U (C), and sunlight KMnO$_4$@PAO-U (D). XPS survey spectra (E), O 1s (F), U 4f (G), and Mn 2p (H) of PAO-U and KMnO$_4$@PAO.

KMnO$_4$@PAO with photo-thermal conversion properties, and significantly increases the temperature of simulated seawater by ∼10 °C just by adding 0.4 g per L KMnO$_4$@PAO under light irradiation conditions (2 h, 0.20 W cm^{-2}). Given the excellent photo-thermal conversion efficiency of KMnO$_4$@PAO, it is expected to be able to overcome seasonal and regional temperature differences and maintain high U(VI) recovery efficiency from seawater. The superb adsorption capability for U(VI), repeatability, and stability of KMnO$_4$@PAO further highlight its application in extraction of U(VI) from seawater.

Conclusions

Experimental section

Synthesis of PAO and KMnO$_4$@PAO. After 3.20 g NH$_2$-OH·HCl and 1.75 g NaOH were dissolved in 20 mL ultrapure water, specific amounts of KMnO$_4$ and PAN were added. The above suspension was reacted at 75 °C in a N$_2$ atmosphere for 7 h, and repeatedly washed with ultrapure water. After drying at 75 °C in a vacuum oven, KMnO$_4$@PAO with different mass ratios was obtained. To evaluate the effect of KMnO$_4$, PAO was also synthesized by the same method. The mass of PAN and KMnO$_4$ in the solution is shown in Table S1.†

Characterization. Fourier transform infrared (FT-IR) spectroscopy was obtained on a Thermo Scientific Nicolet iS5 in transmission mode. Scanning electron microscopy (SEM) and energy dispersive spectrometer (EDS) mapping were adopted to analyse the morphology on an FEI Quanta 250 FEG. X-ray photoelectron spectroscopy (XPS) measurement was carried out with an ESCALab220i-XL surface microanalysis system (VG Scientific) equipped with an Al Kα ($h\lambda$ = 1486.6 eV) source at a chamber pressure of 3 × 10^{-9} mbar, and the surface charging effect was corrected with the C 1s peak at 284.8 eV as a reference. Dynamic light scattering (DLS) measurement was conducted on a Malvern Instruments Zetasizer operated in backscatter (173°) mode.

U(VI) adsorption. The batch adsorption technique was adopted to study the adsorption capability of KMnO$_4$@PAO for U(VI). After KMnO$_4$@PAO was pre-balanced with salinity (such as NaCl) for 24 h, U(VI) solution and de-ionized water were added to achieve the desired compositions, and NaOH or HCl were also used to adjust suspension pH values. After oscillation in an incubator for the desired time, the suspensions were centrifuged at 10 000 rpm for 10 min and filtered by using a 0.22 μm membrane filter. The final U(VI) concentrations (mg L^{-1} and μg L^{-1} levels) in supernatants were measured on an Optima 2100 DV inductively coupled plasma (ICP) atomic emission spectroscopy system (PerkinElmer) and on an ICP mass spectroscopy (ICP-MS, Thermo Scientific X-Series II) system, respectively.

Co-existing metal ion experiment. Several typical metal ions including K(I), Ca(II), Cu(II), Ni(II), Fe(III) and V(V) were selected to verify the influence of coexisting cations on the performance of KMnO$_4$@PAO in recovering U(VI). The compounds of the above cations and $UO_2(NO_3)_2 \cdot 6H_2O$ were used to prepare 10 mg L^{-1} mixed solution. Then 0.020 g KMnO$_4$@PAO was added to 50 mL solutions and the pH value was adjusted. After shaking for 24 h, the final suspensions were filtered with a 0.22 μm membrane filter. The residual U(VI) ion concentration in solution was measured by the ICP-MS method.

Photo-thermal conversion experiment. 0.020 g KMnO$_4$@PAO and 50 mL 20.0 mg per L U(VI) were irradiated by using a 300 W xenon lamp under continuous stirring. The simulated sunlight intensity was measured to be 0.20 W cm^{-2}. The temperature was measured by using an infrared thermal imager (FLIR E60 US FLIR Company).

Conflicts of interest

There are no conflicts to declare.

Acknowledgements

We gratefully acknowledge financial support from the National Natural Science Foundation of China (21976089, 22176098, and 22206081).

Notes and references

1 B. K. Sovacool, P. Schmid, A. Stirling, G. Walter and G. M. Kerron, *Nat. Energy*, 2020, **5**, 928–935.
2 A. Singh, S. Lal, N. Kumar, R. Yadav and S. Kumari, *Environ. Sci. Pollut. Res.*, 2023, **30**, 46185–46203.

3 L. Zhu, C. Zhang, F. Qin, F. Ma, C. Bi, R. Zhu, L. Liu, J. W. Bai, H. Dong and T. Satoh, *J. Mol. Liq.*, 2022, **368**, 120741.

4 J. Yu, H. Zhang, Q. Liu, J. Zhu, J. Yu, G. Sun, R. Li and J. Wang, *J. Hazard. Mater.*, 2022, **440**, 129735.

5 H. B. Pan, C. M. Wai, L. J. Kuo, G. Gill, G. Tian, L. Rao, S. Das, R. T. Mayes and C. J. Janke, *ChemistrySelect*, 2017, **2**, 3769–3774.

6 J. Zhu, Y. Luo, J. Wang, J. Yu, Q. Liu, J. Liu, R. Chen, P. Liu and J. Wang, *J. Mol. Liq.*, 2022, **368**, 120744.

7 A. S. Ivanov, C. J. Leggett, B. F. Parker, Z. Zhang, J. Arnold, S. Dai, C. W. Abney, V. S. Bryantsev and L. Rao, *Nat. Commun.*, 2017, **8**, 1560.

8 I. Tokarev and E. Yakovlev, *Water*, 2021, **13**, 3514.

9 P. Ilaiyaraja, A. K. S. Deb, K. Sivasubramanian, D. Ponraju and B. Venkatraman, *J. Hazard. Mater.*, 2013, **250**, 155–166.

10 C. W. Abney, R. T. Mayes, T. Saito and S. Dai, *Chem. Rev.*, 2017, **117**, 13935–14013.

11 H. B. Pan, L. J. Kuo, C. M. Wai, N. Miyamoto, R. Joshi, J. R. Wood, J. E. Strivens, C. J. Janke, Y. Oyola, S. Das, R. T. Mayes and G. A. Gill, *Ind. Eng. Chem. Res.*, 2016, **55**, 4313–4320.

12 T. Liu, X. Zhang, H. Wang, M. Chen, Y. Yuan, R. Zhang, Z. Xie, Y. Liu, H. Zhang and N. Wang, *Chem. Eng. J.*, 2021, **412**, 128700.

13 H. B. Pan, L. J. Kuo, C. M. Wai, N. Miyamoto, R. Joshi, J. R. Wood, J. E. Strivens, C. J. Janke, Y. Oyola, S. Das, R. T. Mayes and G. A. Gill, *Ind. Eng. Chem. Res.*, 2016, **55**, 4313–4320.

14 Z. Wang, Q. Meng, R. Ma, Z. Wang, Y. Yang, H. Sha, X. Ma, X. Ruan, X. Zou, Y. Yuan and G. Zhu, *Chem*, 2020, **6**, 1683–1691.

15 Y. Wang, Z. Lin, Q. Liu, J. Zhu, J. Liu, J. Yu, R. Chen, P. Liu and J. Wang, *Chem. Eng. J.*, 2021, **425**, 131538.

16 C. Bi, C. Zhang, W. Xu, F. Ma, L. Zhu, R. Zhu, Q. Qi, L. Liu, J. Bai and H. Dong, *Desalination*, 2023, **545**, 116169.

17 Y. Wang, Z. Lin, J. Yu, J. Zhu, J. Liu, Q. Liu, R. Chen, P. Liu and J. Wang, *J. Environ. Chem. Eng.*, 2023, **11**, 109277.

18 H. B. Pan, C. M. Wai, L. J. Kuo, G. A. Gill, J. S. Wang, R. Joshi and C. J. Janke, *Dalton Trans.*, 2020, **49**, 2803–2810.

19 H. B. Pan, L. J. Kuo, J. Wood, J. Strivens, G. A. Gill, C. J. Janke and C. M. Wai, *RSC Adv.*, 2015, **5**, 100715–100721.

20 Q. Chen, X. Xue, Y. Liu, A. Guo, K. Chen, J. Yin, F. Yu, H. Zhu and X. Guo, *J. Hazard. Mater.*, 2022, **438**, 129524.

21 X. Guo, Y. Wang, X. Li, P. Huai and G. Wu, *Mol. Phys.*, 2015, **113**, 1327–1336.

22 J. Kim, C. Tsouris, R. T. Mayes, Y. Oyola, T. Saito, C. J. Janke, S. Dai, E. Schneider and D. Sachde, *Sep. Sci. Technol.*, 2013, **48**, 367–387.

23 D. Zhang, L. Liu, B. Zhao, X. Wang, H. Pang and S. Yu, *Environ. Pollut.*, 2023, **317**, 120826.

24 G. A. Gill, L. J. Kuo, C. J. Janke, J. Park, R. T. Jeters, G. T. Bonheyo, H. B. Pan, C. Wai, T. Khangaonkar, L. Bianucci, J. R. Wood, G. W. Marvin, S. Peterson, G. Abrecht, R. T. Mayes, C. Tsouris, Y. Oyola, J. E. Strivens, N. J. Schlafer, R. S. Addleman, W. Chouyyok, S. Das, J. Kim, K. Buesseler, C. Breier and E. D. Alessandro, *Ind. Eng. Chem. Res.*, 2016, **55**, 4264–4277.

25 L. J. Kuo, H. B. Pan, C. M. Wai, M. F. Byers, E. Schneider, J. E. Strivens, C. J. Janke, S. Das, R. T. Mayes, J. R. Wood, N. Schlafer and G. A. Gill, *Ind. Eng. Chem. Res.*, 2017, **56**, 11603–11611.

26 L. J. Kuo, G. A. Gill, C. Tsouris, L. Rao, H. B. Pan, C. M. Wai, C. J. Janke, J. E. Strivens, J. R. Wood, N. Schlafer and E. K. D. Alessandro, *ChemistrySelect*, 2018, **3**, 843–848.

27 Z. Mi, D. Zhang, J. Wang, S. Bi, J. Liu, X. Gao, D. Zhang, Y. Jiang, Z. Li, Y. Zhu and Z. Liu, *New J. Chem.*, 2022, **46**, 6296–6306.

28 C. C. Wan, R. Yu, L. Meng, D. Wang, T. Duan and L. Li, *Desalination*, 2020, **486**, 114447.

29 S. Shi, R. Wu, S. Meng, G. Xiao, C. Ma, G. Yang and N. Wang, *J. Hazard. Mater.*, 2022, **436**, 128983.

30 S. Lu, L. Chen, M. F. Hamza, C. He, X. Wang, Y. Wei and E. Guibal, *Chem. Eng. J.*, 2019, **368**, 459–473.

31 T. Liu, R. Zhang, M. Chen, Yi. Liu, Z. Xie, S. Tang, Y. Yuan and N. Wang, *Adv. Funct. Mater.*, 2022, **32**, 211104.

32 Y. Yue, B. Wang, X. Xu, D. Cai, L. Zhang, S. Hu, J. Xiao, T. Yang, D. Wang and H. Wu, *Mater. Today Chem.*, 2022, **26**, 101090.

33 C. Han, Y. Yue, X. Xu, D. Cai, Z. Liu, S. Chen, L. Luo, J. Xiao and D. Wang, *New J. Chem.*, 2020, **44**, 19445–19449.

34 H. Heshmati, H. G. Gilani, M. T. Mostaedi and A. Haidary, *J. Dispersion Sci. Technol.*, 2014, **35**, 501–509.

35 S. Wang, G. Yuan, J. Yang, J. Bai, G. Wang and J. Yan, *ChemSusChem*, 2022, **15**, 1–13.

36 D. Shao, G. Hou, F. Chi, X. Lu and X. Ren, *RSC Adv.*, 2021, **11**, 1909–1915.

37 X. Li, J. Huang, Z. Shi, Y. Xie, Z. Xu, J. Long, G. Song, Y. Wang, G. Zhang, X. Luo, P. Zhang, S. Zha and H. Li, *J. Environ. Manage.*, 2023, **342**, 118088.

38 X. Zhang, L. Zhang, Y. Liu, M. Li, X. Wu, T. Jiang, C. Chen and Y. Peng, *Environ. Pollut.*, 2020, **262**, 114841.

39 H. Zhou, J. Yu, S. Liu, L. Wang and P. Li, *Mater. Lett.*, 2023, **333**, 133652.

40 Z. Guo, Y. Liu, Y. Zhang, X. Sun, F. Li, T. Bu, Q. Wang and L. Wang, *Biomater. Sci.*, 2020, **8**, 4266.

41 M. Wen, X. Liu, N. Yu, P. Qiu, D. K. Macharia, M. Li, H. Zhang, Z. Chen and W. Lian, *J. Colloid Interface Sci.*, 2022, **626**, 77–88.